

PACS numbers: 42.55.Px; 42.60.Da; 42.82.Gw
DOI: 10.1070/QE2015v045n12ABEH015871

Integrated high-order surface diffraction gratings for diode lasers

V.V. Zolotarev, A.Yu. Leshko, N.A. Pikhtin, S.O. Slipchenko,
Z.N. Sokolova, Ya. V. Lubyanskiy, N.V. Voronkova, I.S. Tarasov

Abstract. **High-order surface diffraction gratings acting as a distributed Bragg reflector (DBR) in mesa stripe semiconductor lasers (λ = 1030 nm) have been studied theoretically and experimentally. Higher order interfering radiation modes (IRMs), which propagate off the plane of the waveguide, have been shown to have a crucial effect on the reflection and transmission spectra of the DBR. The decrease in the reflectivity of the DBR in response to the increase in the diffraction efficiency of these modes may reach 80 % and more. According to theoretical analysis results, the intensity of the higher order IRMs is determined by the geometry of the DBR groove profile. Experimental data demonstrate that the noncavity modes are responsible for parasitic light leakage losses in the laser cavity. It has been shown that, in the case of nonoptimal geometry of the grating groove profile, the overall external differential quantum efficiency of the parasitic laser emission may exceed 45 %, which is more than half of the laser output power. The optimal geometry of the DBR groove profile is trapezoidal, with the smallest possible lower base. Experimental evidence has been presented that this geometry considerably reduces the power of the higher order IRMs and minimises the parasitic light leakage loss.**

Keywords: *semiconductor lasers, distributed feedback, Bragg gratings.*

1. Introduction

A semiconductor laser with a distributed Bragg reflector (DBR) or distributed feedback (DFB) is a key element of integrated optoelectronics. Basic to such a laser is a distributed dispersive component – Bragg diffraction grating (BDG). The fabrication of a buried integrated BDG complicates the process of making a semiconductor laser [1], because BDG formation and epitaxial overgrowth are processes of increased complexity. Therefore, the necessity of raising the spectral density of the emission from semiconductor light sources, especially in the case of high-power semiconductor lasers, requires a search for novel technological approaches. The modern principle of making BDGs is to produce surface dispersive elements for both single-mode [2] and multimode [3, 4] semiconductor lasers. This allows one to pass to a simpler technology and extend the possibilities of the topology of a semiconductor laser as an integrated element. Another component of the concept of a surface BDG is the use of high orders of diffraction, which significantly facilitates the grating fabrication process and reduces its cost [5, 6]. At the same time, the use of high-order surface BDGs gives rise to new distinctive features, both positive and negative.

In this paper, we present a theoretical and experimental study of the properties of a high-order Bragg diffraction grating produced by reactive ion etching on the surface of a separate-confinement laser heterostructure based on AlGaAs/GaAs/InGaAs solid solutions.

2. Calculational model for a high-order surface BDG

The basic characteristics of a surface diffraction grating acting as a DBR are its reflection and transmission spectra, whose shape and behaviour depend on the waveguide design; diffraction order N, which appears in the Bragg condition

$$\Lambda = N\lambda/2n_{\text{eff}} \tag{1}$$

(where Λ is the DBR period; n_{eff} is the effective refractive index of the dielectric medium; and λ is the incident light wavelength); and the geometry of a single DBR groove.

Here we consider a planar dielectric waveguide with a periodically varying refractive index in one of its cladding layers (Fig. 1). The waveguide is a component of a laser heterostructure based on AlGaAs/GaAs/InGaAs solid solutions. The periodic variation in refractive index is produced in the top emitter layer of the heterostructure by reactive ion etch-

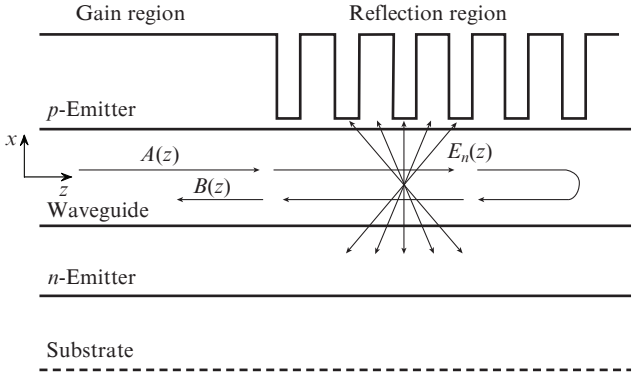

Figure 1. Schematic of a planar dielectric waveguide with a surface DBR.

V.V. Zolotarev, A.Yu. Leshko, N.A. Pikhtin, S.O. Slipchenko, Z.N. Sokolova, Ya. V. Lubyanskiy, N.V. Voronkova, I.S. Tarasov Ioffe Physical Technical Institute, Russian Academy of Sciences, Politekhnicheskaya ul. 26, 194021 St. Petersburg, Russia; e-mail: zolotarev.bazil@mail.ioffe.ru

Received 4 June 2015; revision received 31 August 2015
Kvantovaya Elektronika **45** (12) 1091 – 1097 (2015)
Translated by O.M. Tsarev

ing. The inhomogeneity period is ~1 μm, which allows a standard photolithography process to be used. This period ensures a high order of diffraction ($N \gg 1$) at a light wavelength $\lambda \approx 1.06$ μm, corresponding to the laser heterostructure. The diffraction grating region is passive and electrically isolated from the region where the current flows. Thus, the Bragg diffraction grating is a passive DBR only due to the periodicity of the real part of the refractive index.

The calculational model presented below allows one to analyse systems with a nonuniform refractive index and gain for various resonator configurations (DBR or DFB).

Characteristically, in the case of an electromagnetic wave propagating in a planar dielectric waveguide with a periodically varying refractive index, there are preferential directions for the interference of the light that has diffracted from each boundary of the inhomogeneity [7]. The spatial propagation direction of the jth beam is determined by the relation

$$\Phi_j = 90° + \arcsin(2j/N - 1), \tag{2}$$

where $|2j/N - 1| \leqslant 1$. Thus, for first-order diffraction ($N = 1$) there are two beams propagating in the plane of the waveguide in the $\pm z$ directions [$A(z)$ and $B(z)$ resonator modes in Fig. 1]. In the case of a Bragg element with an order of diffraction $N > 1$, electromagnetic radiation can propagate in directions that lie out of the plane of the waveguide [interfering radiation modes (IRMs) of higher order diffraction: $E_n(x, z)$ in Fig. 1]. Note that there are always two modes parallel to the z axis. The reflection spectrum of a DBR is determined by the ratio of the amplitudes of the reflected ($\Phi = 180°$) and incident ($\Phi = 0$) waves: $B(z)/A(z)$.

Coupled-mode theory, which describes the distribution of an electromagnetic wave in a periodic waveguide, was first proposed by Kogelnik and Shank [8] and Yariv [9]. We will use this theory in the following approximations: the electromagnetic radiation has only a TE polarisation and the E vector lies in a lateral plane along the y axis (hereafter, the subscript y will be omitted). The structure is taken to be infinite in the lateral direction, which is due to the large width of the stripe contact, W ($W \gg \lambda/n_{\text{eff}}$), i.e. $E_y(x, y, z) \equiv E(x, z)$.

The coupled-mode problem reduces to finding a solution to the steady-state wave equation

$$\nabla^2 E(x,z) + k_0^2[\varepsilon(x) + \Delta\varepsilon(x,z)]E(x,z) = 0, \tag{3}$$

were k_0 is the wave vector in vacuum; $\varepsilon(x)$ is the effective dielectric permittivity of the waveguide; and $\Delta\varepsilon(x, z)$ is a periodic dielectric permittivity nonuniformity. The following relations are valid for the nonuniformity under examination:

$$\Delta\varepsilon(x,z) = \Delta\varepsilon(x, z + \Lambda),$$

$$\Delta\varepsilon(x,z) = \sum_{m \neq 0} \Delta\varepsilon_m(x) \exp\left(\frac{\mathrm{i}2\pi}{\Lambda} mz\right). \tag{4}$$

The terms in the expansion of the periodic dielectric permittivity function are determined by the geometry of a single BDG groove:

$$\Delta\varepsilon_m(x) = \frac{n_2^2 - n_1^2}{\mathrm{i}2\pi m} \times \left[\exp\left(\frac{-\mathrm{i}2\pi m}{\Lambda} w_2(x)\right) - \exp\left(\frac{-\mathrm{i}2\pi m}{\Lambda} w_1(x)\right)\right]. \tag{5}$$

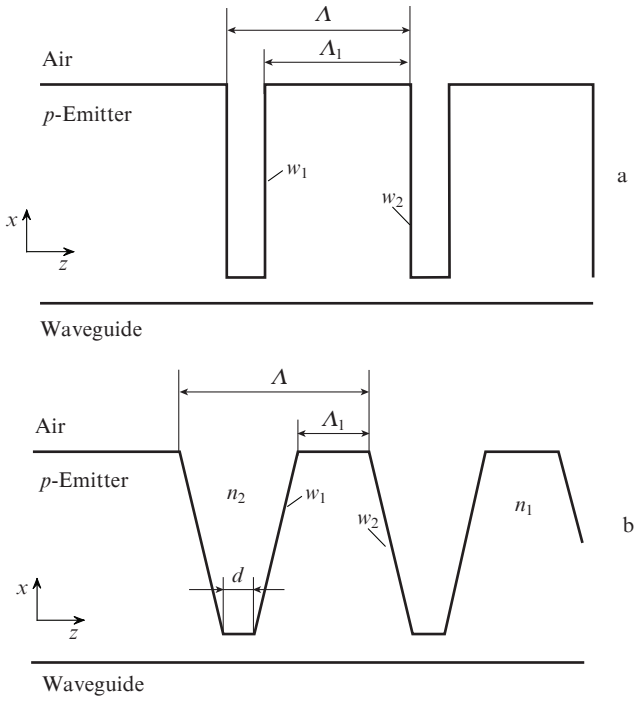

Figure 2. Schematic diagrams of DBRs with (a) rectangular and (b) trapezoidal groove profiles.

Here, the functions $w_1(x)$ and $w_2(x)$ describe the shape of the left- and right-hand faces of the grating grooves, respectively, and n_1 and n_2 are the respective refractive indices (Fig. 2).

The solution to Eqn (3) is the function [10]

$$E(x,z) = U(x)[A(z)\exp(\mathrm{i}\beta_0 z) + B(z)\exp(-\mathrm{i}\beta_0 z)] + \sum_{n=1}^{N-1} E_n(x,z)\exp\left(\mathrm{i}\frac{N-2n}{\Lambda}\pi z\right), \tag{6}$$

where $U(x)$ is the electromagnetic field distribution along the normal to the plane of the waveguide (guided mode configuration; TE_0 in our case); $A(z)$ and $B(z)$ are the electromagnetic radiation amplitudes along the resonator axis (resonator modes); and $\beta_0 = \pi N/\Lambda$ is the wave vector of the Bragg grating. The last term in (6) describes higher order IRMs which propagate beyond the waveguide at their own angles to the resonator axis according to (2). The number of such modes is $N-1$.

Substituting (6) into (3) and taking into account that $A(z)$, $B(z)$ and $E_n(x,z)$ vary little along the z axis [$\mathrm{d}^2(A, B, E_n)/\mathrm{d}z^2 = 0$], we obtain a system of coupled differential equations in the amplitudes $A(z)$ and $B(z)$:

$$\frac{\mathrm{d}A}{\mathrm{d}z} = \mathrm{i}(\Delta\beta - \mathrm{i}\kappa_\beta^A)A + \mathrm{i}(\kappa + \mathrm{i}\kappa_{\text{coup}}^{BA})B,$$

$$-\frac{\mathrm{d}B}{\mathrm{d}z} = \mathrm{i}(\Delta\beta - \mathrm{i}\kappa_\beta^B)B + \mathrm{i}(\kappa + \mathrm{i}\kappa_{\text{coup}}^{AB})A, \tag{7}$$

where $\Delta\beta = \beta - \beta_0 = [(2\pi/\lambda)n_{\text{eff}} + \mathrm{i}\alpha] - N\pi/\Lambda$ is the difference of the wave vectors of the light and DBR; $\alpha > 0$ is the internal optical loss in the laser heterostructure; and

$$\kappa = \frac{k_0^2}{2\beta}\frac{\int \Delta\varepsilon_N(x)\,U^2(x)\,\mathrm{d}x}{\int U^2(x)\,\mathrm{d}x} \tag{8}$$

is referred to as the coupling coefficient. In the Fourier series (4), a major contribution to exchange interaction is only made by the term whose number corresponds to the order of diffraction, N, in the Bragg condition. It is this constant that determines the magnitude of direct interaction between the resonator modes $A(z)$ and $B(z)$.

The correction coefficients κ_β^A, κ_β^B, $\kappa_{\text{coup}}^{AB}$ and $\kappa_{\text{coup}}^{BA}$ are determined by the solution to the wave equation in $E_n(x, z)$. In the case of purely real coupling ($\kappa = \kappa^*$ and, hence, there is no periodic gain nonuniformity) and a symmetric profile of the DBR grooves [$w_1(x) = w_2(-x)$ in (5)], the following relations are valid: $\kappa_\beta^A = \kappa_\beta^B \equiv \kappa_\beta$ and $\kappa_{\text{coup}}^{AB} = \kappa_{\text{coup}}^{BA} \equiv \kappa_{\text{coup}}$.

Shams-Zadeh-Amiri et al. [11] determined these constants using the Green's function for the solution to the wave equation in $E_n(x, z)$:

$$\kappa_\beta = \sum_{n=1}^{N-1} K_{(n,N-n)},\quad \kappa_{\text{coup}} = \sum_{n=1}^{N-1} K_{(n,-n)},\quad K_{(u,v)} = \frac{\mathrm{i}k_0^3}{2n_{\text{eff}}}$$
$$\times \iint \Delta\varepsilon_u(x)\,\Delta\varepsilon_v(x')\,U(x)\,U(x')\,G_{|v|}(x,x')\,\mathrm{d}x\mathrm{d}x', \tag{9}$$

where $G_\tau(x, x')$ is the Green's function for the equation

$$\frac{\partial^2 G_\tau(x,x')}{\partial x^2} + \left[\varepsilon k_0^2 - \frac{(N-2\tau)^2\pi^2}{\Lambda^2}\right] G_\tau(x,x') = \delta(x-x').$$

The coefficient κ_β characterises the effect of the $A(z)$ and $B(z)$ modes on the $E_n(x, z)$ higher order noncavity IRMs, with $\mathrm{Re}(\kappa_\beta) < 0$ determining the light leakage loss, i.e. the fraction of the power brought away from the laser cavity by the higher order IRMs, and $\mathrm{Im}(\kappa_\beta)$ being the shift of the peak in the reflection spectrum with respect to the Bragg condition (1). The coefficient κ_{coup} characterises the indirect exchange interaction between the $A(z)$ and $B(z)$ modes through the higher order IRMs.

It is important to note that the presence of the coefficients κ_β and κ_{coup} is the result of taking into account the higher order IRMs. To perform a comparative analysis, below we present numerical calculation results for two cases. In one case, we neglect the higher order IRMs in solving (6), i.e. we take $E_n(x, z) = 0$ and, accordingly, $\kappa_\beta = \kappa_{\text{coup}} = 0$. In the other case, we find a solution to the wave equation with $E_n(x, z) \neq 0$.

Relations (8) and (9) include terms form the Fourier series (4), which depend on the geometry of the DBR grooves. Therefore, the groove profile has a direct effect on both the rate of energy exchange between resonator modes and the energy loss from the resonator through the higher order IRMs.

A detailed solution to system (7) was presented previously [10–12], so we here determine only the reflectivity of the DBR subject to the following boundary conditions: (1) a wave is incident on the DBR at point $z = 0$ and has an amplitude $A(0)$; (2) the length of the DBR is L and there is no reflection from the end facet at $z = L$. Thus, the $B(z)$ mode is only due to exchange interaction [$B(L) = 0$]. Under these boundary conditions, the reflectance and transmittance of the DBR are given by

$$r_{\text{DBR}} = B(0)/A(0),\quad R_{\text{DBR}} = |r_{\text{DBR}}|^2,$$
$$t_{\text{DBR}} = A(L)/A(0),\quad T_{\text{DBR}} = |t_{\text{DBR}}|^2. \tag{10}$$

3. Properties of a high-order surface BDG

Calculations were performed in the above model for an $Al_{0.25}Ga_{0.75}As/Al_{0.1}Ga_{0.9}As/Al_{0.25}Ga_{0.75}As$ waveguide 1.7 μm in thickness. The DBR period Λ was 2.4 μm, which corresponds to $N = 16$ at a wavelength $\lambda \approx 1030$ nm. The grating depth was 0.1 μm less than the emitter thickness. The choice of the geometry of the grating was dictated by grating fabrication process conditions. Given the potentialities of reactive ion etching, we chose rectangular and trapezoidal groove profiles (Fig. 2).

Figure 3a shows typical reflection and transmission spectra of DBRs with no allowance for higher order IRMs. The maximum reflectivity is only limited by the internal optical loss in the heterostructure (at a sufficient grating length). The peak-reflection wavelength coincides with the Bragg resonance wavelength in (1). Analysis with allowance for higher order IRMs (Fig. 3b) leads to changes in the shape of the spectra and their extreme values. In this case, the peak-reflection wavelength shifts with respect to the Bragg wavelength, and the intensity of light in the transmission spectrum decreases. These features are the result of taking into account the external optical energy loss in the higher order IRMs. This contribution is well illustrated by the optical loss in the DBR ($1-R-T$) (Fig. 3c). With no allowance for higher order IRMs, there is no loss in the DBR and $R + T = 1$ (Fig. 3c, solid line). When noncavity modes are taken into account, we have $1-R-T > 0$ (Fig. 3c, dashed line), which can be accounted for by the external optical power loss.

As pointed out above, the defining factor of the exchange interaction of higher modes with the $A(z)$ and $B(z)$ resonator modes is the geometry of the grating grooves. To assess this effect, we calculated the reflectivity of rectangular and trapezoidal DBRs with different geometric parameters.

Figure 4a shows the peak reflectivity in the spectrum of a DBR as a function of the grating duty cycle $D = \Lambda_1/\Lambda$ (see Fig. 2a) in the case of a rectangular groove profile. The dashed line represents calculation results obtained with no allowance for higher order IRMs. The spectrum has zero-reflectance points, which correspond to the maximum transmission of the DBR. Note that the maximum attainable reflection peaks (maxima in this graph) are identical in height. The number of peak-reflection points corresponds to an order of Bragg diffraction $N = 16$. The solid line in Fig. 4a represents analogous data obtained with allowance for higher order IRMs. In addition to zero-reflectance points, we observe a decrease in the reflectivity of the DBR, especially in the vicinity of $D = 50\%$. The maximum R corresponds to the maximum grating duty cycle and is determined by the window in the photoresist mask. The calculation results suggest that, to obtain a high-reflectivity DBR, one should control the groove profile and reduce the size of the etch region. A photolithography process is incapable of producing a window ~100 nm in size, which makes it impossible to achieve the maximum reflectivity. In view of this, we performed calculations for a trapezoidal groove profile in a DBR (see Fig. 2b).

Figure 4b shows the peak reflectivity as a function of the base width d of the etch region for a trapezoidal groove pro-

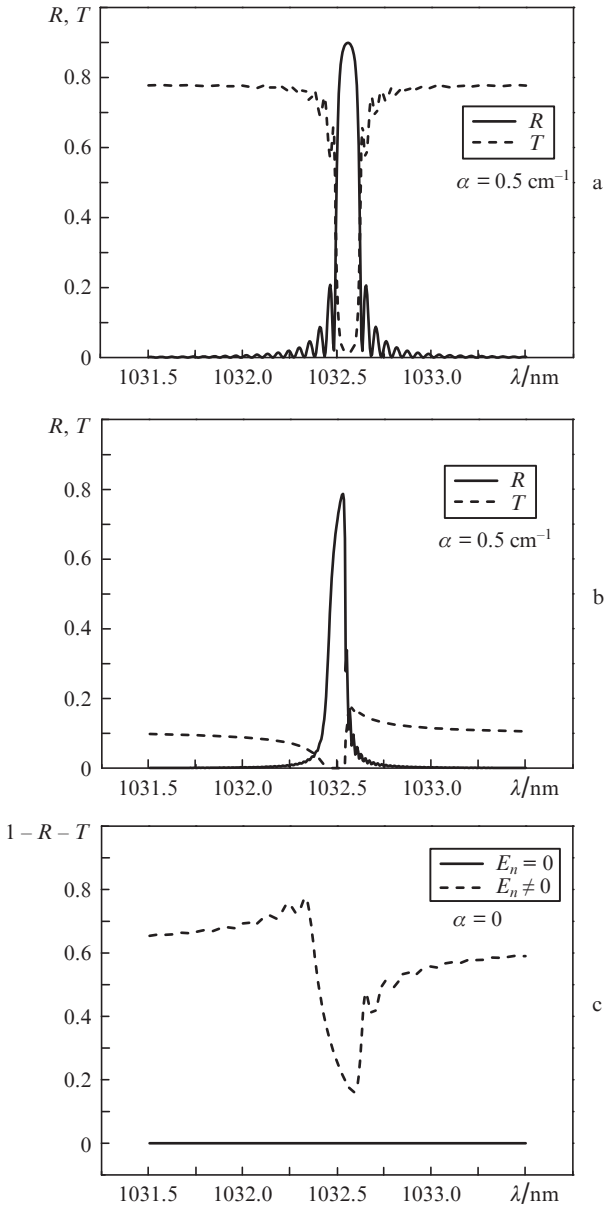

Figure 3. Calculated reflection and transmission spectra of DBRs (a) without and (b) with allowance for higher order IRMs; (c) calculated loss spectra of a zero internal loss DBR in a laser heterostructure.

file. The number of peaks is here a factor of 2 smaller. When the higher order IRMs are taken into account, at a given length Λ_1 of the upper base of the groove profile (which is determined by the photoresist mask) changing the geometry of the groove walls from sawtooth ($d = 0$) to vertical ($d = \Lambda - \Lambda_1$) reduces R. Thus, to obtain a high-reflectivity DBR by a standard fabrication process, one should use a trapezoidal groove profile and minimise the length of the lower base, d, of the groove profile.

The reduction in the reflectivity of DBRs is related to the power of the higher order IRMs, E_n. An increase in it leads to an increase in light leakage from the resonator. Figure 5 shows the light leakage loss due to the higher order IRMs [$-2\mathrm{Re}(\kappa_\beta)$] as a function of grating duty cycle D for a rectangular groove profile. At $\Lambda_1 = \Lambda/2$ ($D = 50\%$), the loss has a maximum and, accordingly, the reflectivity of the DBR has a minimum (Fig. 4a). The reduction in R is caused by the increase in the diffraction efficiency of the DBR for the interfering modes, so optical power predominantly leaks from the resonator off the plane of the waveguide.

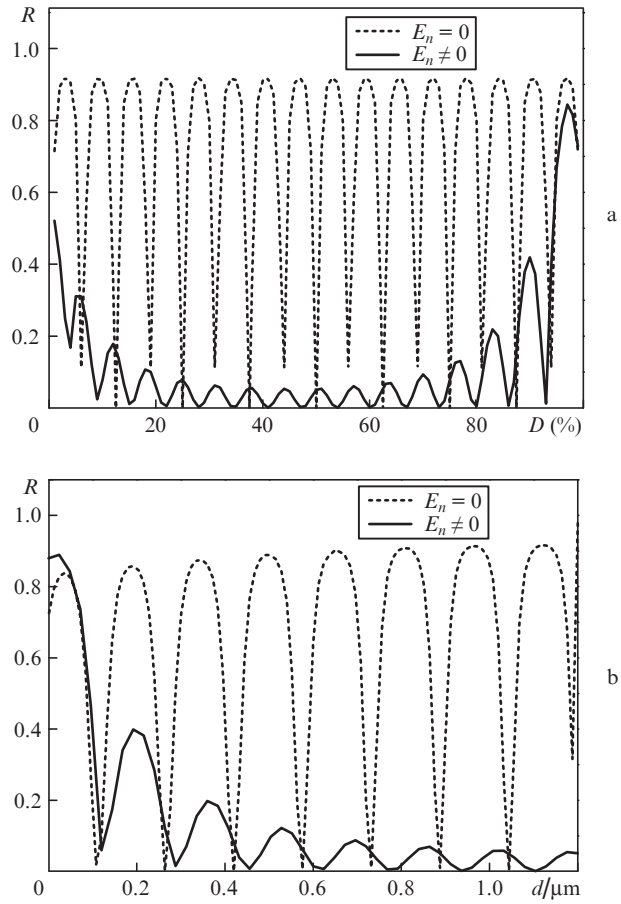

Figure 4. Calculated peak reflectivity as a function of the geometric parameters of DBR grooves for (a) rectangular and (b) trapezoidal groove profiles.

Calculation results demonstrate that the shape of the DBR groove profile determines the power distribution between all (cavity and noncavity) modes. Thus, at a given DBR period and given waveguide parameters, varying the

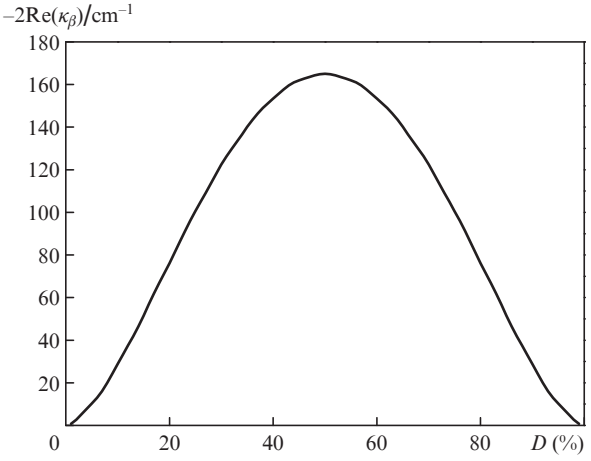

Figure 5. Calculated real part of the correction coupling coefficient κ_β (which determines the external optical loss of DBRs) as a function of grating duty cycle D for a rectangular groove profile.

shape of the groove profile allows one to control the optical power at the resonator output.

4. Experimental study of the properties of a high-order surface BDG

Experimental samples had the form of a DBR laser. The laser was based on a separate-confinement double heterostructure in the AlGaAs/GaAs/InGaAs solid-solution system and comprised two sections. The gain section had a standard mesa stripe design with an Ohmic contact. The width of the gain region was $W = 100$ μm and its length was 3 mm. The reflection section was electrically passive and its length was 1 mm. The end facets of the resonator were naturally cleaved. The samples were mounted on copper heatsinks using both *p*- and *n*-contacts. The grating had a trapezoidal groove profile with a base width $d = 0.35$ μm (Fig. 6a). We examined lasers with a DBR period of 2.4 and 3.5 μm.

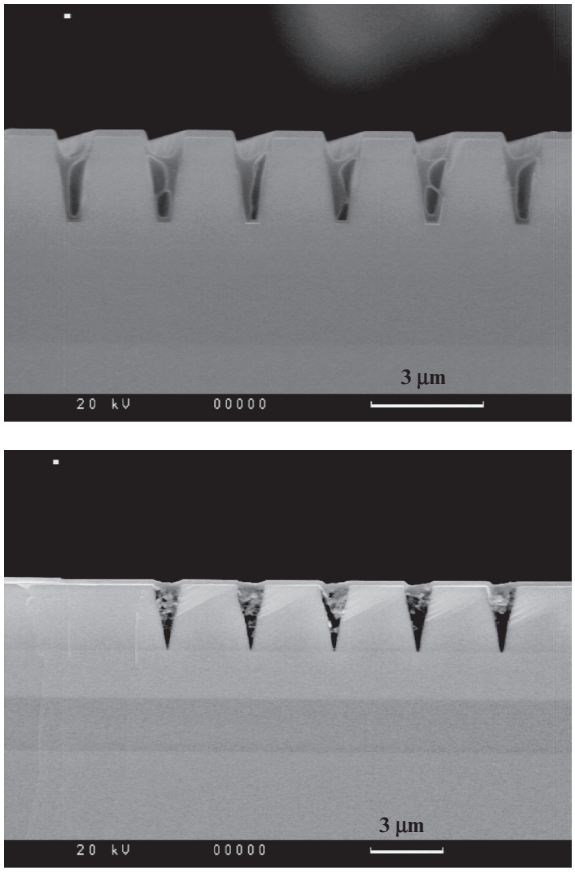

Figure 6. Electron-microscopic images of surface DBRs: (a) grating period $\Lambda = 2.4$ μm, base width $d = 0.35$ μm; (b) $\Lambda = 3.5$ μm, $d < 0.05$ μm.

We measured emission spectra and light–current characteristics of the end facet of the resonator on the side of the gain region. In addition, we assessed the internal optical loss in the laser heterostructure, which was determined to be 0.5 cm^{-1}. The laser output spectrum corresponded to the Bragg condition for $\lambda \approx 1032$ nm, with a bandwidth $\delta\lambda < 0.2$ nm. The external differential efficiency of the lasers was 25%.

To investigate higher order IRMs, we measured the radiation pattern in a wide angular range. Figure 7 shows a far-field pattern of DBR lasers mounted with their *p*-emitter up, with $N = 16$ ($\Lambda = 2.4$ μm). The broad peak at $\Phi = 0$ corresponds to emission from the end facet of the laser on the side of the gain region. On the opposite side of the laser ($\Phi = 180°$), emission is negligible. The sharp peaks correspond to emission of higher order interfering modes from the DBR surface. Figure 8 schematically illustrates light propagation according to Eqn (1) at $N = 16$ across the *p*-emitter/air interface of a laser heterostructure. The dashed line represents the angle of total internal reflection. Comparison of Figs 7 and 8 indicates that only those rays propagating at an angle smaller than α_{cr} were observed in our experiments, i.e. only some of the higher order IRMs were observed.

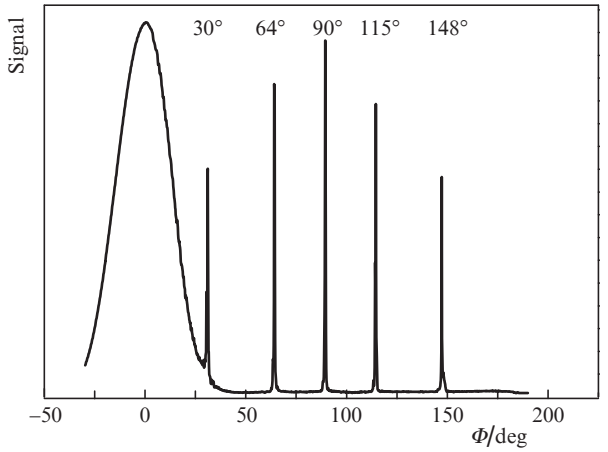

Figure 7. Radiation pattern of a DBR laser.

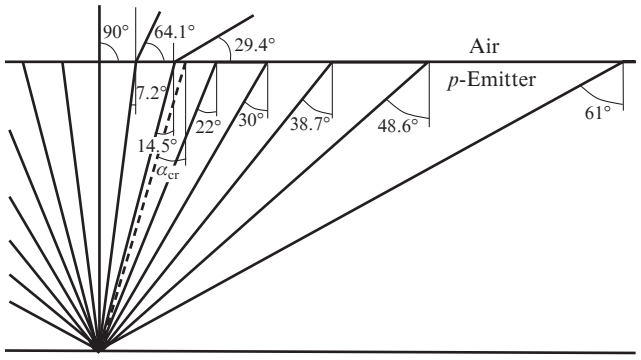

Figure 8. Schematic diagram of the propagation angles of higher order diffracted modes at $N = 16$ (α_{cr} is the angle of total internal reflection).

The far-field measurement results presented in Fig. 7 are characteristic as well of the light passing through the substrate. Therefore, the optical energy is brought away from the laser cavity by $2(N-1)$ rays that characterise the higher order IRMs. Similar experimental data were obtained for an $N = 23$ ($\Lambda = 3.5$ μm) DBR.

The measured spectrum of the higher order modes coincided with the emission spectrum of the end facet of the laser. Figure 9 shows light–current characteristics of the higher order modes ($N = 16$). The external differential quantum efficiency η_{dif} of each mode is about 1%. Since experimental data (Fig. 7) demonstrate that light undergoes refraction on the air–emitter interface, light–current measurements detect only part of the optical power of an interfering mode. The fraction of the interfering mode power reflected from the

interface between the two media reaches 30% to 50% (according to the Fresnel formulas it depends on the angle of incidence). The estimated overall external differential quantum efficiency of all the higher order IRMs is about 45%. Thus, a laser with a trapezoidal DBR groove profile and a base width $d = 0.35$ μm has a light leakage loss above 45%.

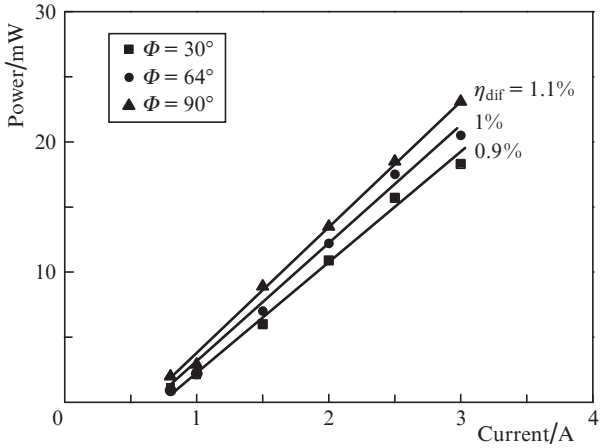

Figure 9. Light–current characteristics of different higher order IRMs detected on the surface of the DBR (see Fig. 7).

Far-field measurements in the lateral direction in the plane of the waveguide showed that there were higher order IRMs propagating in the same direction. Emission in the lateral direction is due to edge effects on the end facets of the DBR grooves on the boundary of the mesa structure. Light propagating in the plane of the waveguide is absorbed in the active region, which makes it impossible to measure its power. It is clear however that the optical power loss in the resonator only increases.

Experimental data for DBR samples with a trapezoidal groove profile and a base width $d < 0.05$ μm (Fig. 6b) demonstrate that far-field patterns of such samples contain characteristic narrow emission bands of the DBR surface. The optical power of the higher order IRMs is comparable to the level of spontaneous emission observed through the grating surface, which makes it impossible to experimentally determine the external differential quantum efficiency of such modes but points to a considerable decrease in the optical loss due to the parasitic emission of the higher order IRMs.

5. Discussion

The experimental data and theoretical results obtained in this study demonstrate that the main cause of losses in the cavity of a DBR laser is the parasitic output emission due to higher order IRMs. The parameter that determines the optical power distribution between the cavity and noncavity modes is the geometry of the grating groove profile. In the case of a rectangular groove profile, high reflectivity ($R > 90\%$) can only be reached by minimising the width of the etch region, which limits the applicability of the photolithography process. A trapezoidal DBR groove profile allows one to reach high reflectivity by minimising the groove base width deep in the etch region for a micron-scale photoresist mask. For this reason, it is a triangular shape of the etch region which is optimal and minimises parasitic light leakage losses.

Experimental power measurements for the higher order IRMs of a DBR with a trapezoidal groove profile and $d = 0.35$ μm showed that these modes accounted for more than half of the laser output power and were responsible for parasitic light leakage losses. It is important to note that the DBR does not increase the internal optical loss in the waveguide. Thus, the use of a DBR with optimal geometry of the groove profile will allow one to create a high-efficiency reflective component of resonators. Our results demonstrate that, in the case of a DBR with a trapezoidal groove profile and the minimum base width ($d = 0.05$ μm), surface mode emission persists, but the parasitic external optical loss drops to a minimum.

6. Conclusions

High-order surface diffraction gratings acting as a distributed Bragg reflector in mesa stripe semiconductor lasers ($\lambda = 1030$ nm) have been studied theoretically and experimentally. It has been shown that taking into account higher order IRMs, which propagate off the plane of the waveguide, plays a key role in determining the reflection and transmission spectra of a DBR. According to theoretical analysis results, the optical power of the higher order IRMs is determined by the geometry of the DBR groove profile. Nonoptimal geometry of the DBR groove profile raises the power of noncavity modes and reduces the reflectivity of the DBR by more than 80%. The latter is due to the increase in diffraction efficiency for the noncavity modes. It is the presence of higher order IRMs, which show up as a set of rays with a low diffraction divergence of emission from the DBR surface, that leads to parasitic light leakage losses in the laser cavity. It has been shown that, in experimental samples with a nonoptimal geometry of the DBR groove profile, the external differential quantum efficiency of the parasitic emission of the higher order IRMs reaches 45%, so the parasitic optical loss accounts for more than half of the laser output power. In the case of DBRs with the most technologically attractive trapezoidal grating groove profile, maximum reflectivity can be reached by minimising the groove base width deep in the etch region, and this geometry minimises the parasitic light leakage loss.

Thus, to obtain a high-reflectivity DBR element, precision control over the geometry of the grating groove profile is required. The presence of higher order radiation modes opens up the possibility of creating a laser with light output through a surface with a low diffraction divergence of emission.

Acknowledgements. This work was supported by the Physical Sciences Division of the Russian Academy of Sciences (Programme No. III-7).

References

1. Nguyen T.-P., Schiemangk M., Spießberger S., Wenzel H., Wicht A., Peters A., Erbert G., Tränkle G. *Appl. Phys. B*, **108**, 767 (2012).
2. Zimmerman J.W., Price R.K., Reddy U., Dias N.L., Coleman J.J. *IEEE J. Sel. Top. Quantum Electron.,* **19**, 1503712 (2013).
3. Zolotarev V.V., Leshko A.Yu., Pikhtin N.A., Lyutetskiy A.V., Slipchenko S.O., Bakhvalov K.V., Lubyanskiy Ya.V., Rastegaeva M.G., Tarasov I.S. *Kvantovaya Elektron.*, **44**, 907 (2014) [*Quantum Electron.*, **44**, 907 (2014)].
4. Fricke J., Bugge F., Ginolas A., John W., Klehr A., Matalla M., Ressel P., Wenzel H., Erbert G. *IEEE Photonics Technol. Lett.*, **22**, 284 (2010).

5. Zolotarev V.V., Leshko A.Yu., Lyutetskiy A.V., Nikolaev D.N., Pikhtin N.A., Podoskin A.A., Slipchenko S.O., Sokolova Z.N., Shamakhov V.V., Arsent'ev I.N., Vavilova I.S., Bakhvalov K.V., Tarasov I.S. *Fiz. Tekh. Poluprovodn.*, **47**, 124 (2013).
6. Fricke J., Wenzel H., Matalla M., Klehr A., Erbert G. *Semicond. Sci. Technol*., **20**, 1149 (2005).
7. Casey H.C., Jr., Panish M.B. *Heterostructure Lasers* (New York: Academic, 1978; Moscow: Mir, 1981).
8. Kogelnik H., Shank C.V. *J. Appl. Phys*., **43**, 2327 (1972).
9. Yariv A. *IEEE J. Quantum Electron*., **9**, 919 (1973).
10. Streifer W., Scifres D., Burnham R.D. *IEEE J. Quantum Electron.*, **13**, 134 (1977).
11. Shams-Zadeh-Amiri A.M., Jin Hong, Xun Li, Huang Wei-Ping. *IEEE J. Quantum Electron*., **36**, 1421 (2000).
12. Wenzel H., Guther R., Shams-Zadeh-Amiri A.M., Bienstman P. *IEEE J. Quantum Electron*., **42**, 64 (2006).